

Enhanced Superexchange in a Tilted Mott Insulator

Ivana Dimitrova¹, Niklas Jepsen¹, Anton Buyskikh², Araceli Venegas-Gomez², Jesse Amato-Grill^{1,3}, Andrew Daley², and Wolfgang Ketterle¹

¹*Department of Physics, Research Laboratory of Electronics, MIT-Harvard Center for Ultracold Atoms, Massachusetts Institute of Technology, Cambridge, Massachusetts 02139, USA*

²*Department of Physics and SUPA, University of Strathclyde, Glasgow G4 0NG, United Kingdom*

³*Department of Physics, Harvard University, Cambridge, Massachusetts 02138, USA*

 (Received 26 August 2019; published 31 January 2020)

In an optical lattice, entropy and mass transport by first-order tunneling are much faster than spin transport via superexchange. Here we show that adding a constant force (tilt) suppresses first-order tunneling, but not spin transport, realizing new features for spin Hamiltonians. Suppression of the superfluid transition can stabilize larger systems with faster spin dynamics. For the first time in a many-body spin system, we vary superexchange rates by over a factor of 100 and tune spin-spin interactions via the tilt. In a tilted lattice, defects are immobile and pure spin dynamics can be studied.

DOI: [10.1103/PhysRevLett.124.043204](https://doi.org/10.1103/PhysRevLett.124.043204)

The importance of spin systems goes far beyond quantum magnetism. Many problems in physics can be mapped onto spin systems. Famous examples are the Jordan-Wigner transformation between spin chains and lattice fermions, and the mapping of neural networks to Ising models. The study of spin Hamiltonians has provided major insights into phase transitions and nonequilibrium physics. Therefore, the properties of well-controlled spin systems are explored using various platforms [1].

In the field of ultracold atoms, such Hamiltonians are realized by a mapping from the Hubbard model with the system in the Mott insulator (MI) to Heisenberg models with effective spin-spin coupling given by a second-order tunneling process (superexchange) [2,3]. Although immense progress has been made toward the realization of spin-ordered ground states [4–7], a major challenge is to reach low spin temperatures. A promising route is adiabatic state preparation [8], but in a trapped system a higher entropy region surrounds a low-entropy MI core, whose ultimate temperature and lifetime is limited in most cases by mass or energy transport. A fundamental limitation of superexchange-driven schemes is that the lattice depth controls both mass transport (occurring at the tunneling rate t/\hbar) and the effective spin dynamics (at $t^2/(\hbar U)$, where U is the on-site interaction). Schemes isolating the MI by shaping the trapping potential have been proposed [9–13].

Here we use a controlled potential energy offset between neighboring sites (a tilt) to decouple spin transport from density dynamics in the MI regime. Tilted lattices have been used before to suppress tunneling (in spin-orbit coupling schemes with laser-assisted tunneling [14–17]) or to implement spin models using resonant tunneling between sites with different occupations [18–21]. Energy offsets have been used in double-well potentials to modify

superexchange rates [22] and between sublattices to suppress first-order tunneling and to observe magnetization decay via superexchange [23].

The implications of using an off-resonant tilt for studying spin physics fall into four categories: (i) A tailored density distribution can be chosen that is frozen in by the tilt. (ii) The tilt suppresses the transition to a superfluid (SF). We use these two features to stabilize larger MI plateaus at lower lattice depths. (iii) The sign and magnitude of the superexchange interaction can be tuned with the tilt, which allows access to a larger range of magnetic phases. (iv) In a tilted MI with n atoms per site, number defects ($n \pm 1$) are localized. This turns $t - J$ models [24] into spin models with static impurities and allows the study of pure spin dynamics.

In a tilted lattice, the energy difference between lattice sites prevents first-order tunneling. More precisely, the dynamics of a single particle are Bloch oscillations [25,26] and if the tilt per site Δ is larger than the bandwidth, their amplitude is smaller than a lattice site. In contrast, swapping particles incurs no energy cost, preserving superexchange (Fig. 1), but with a modified matrix element. For $n = 1$, it is [22]

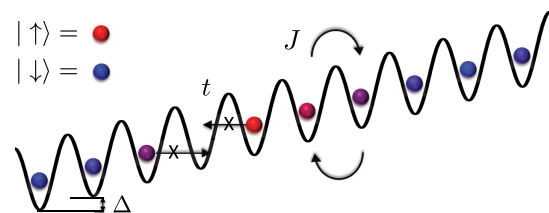


FIG. 1. In a tilted lattice with energy offset per site Δ , tunneling at t/\hbar is suppressed, while superexchange at $J(\Delta)/\hbar$ is still allowed. This enables the slower superexchange processes to dominate the dynamics even in systems with defects.

$$J(\Delta) = \frac{4t^2}{U} \frac{1}{2} \left(\frac{1}{1 - \Delta/U} + \frac{1}{1 + \Delta/U} \right), \quad (1)$$

where tunneling resonances at $\Delta = U/m$ ($m = 1, 2, 3, \dots$) [21] should be avoided. We implement the tilt with an ac Stark shift gradient from a far-detuned 1064 nm laser beam, offset by a beam radius from the sample. We load a ^7Li Bose-Einstein condensate [27] into a 3D 1064 nm optical lattice in the MI regime. Although the tilt can be applied in any direction, here we use a tilt only along one axis of the lattice and study 1D dynamics (see Supplemental Material [28]).

(i) Preparing large nonequilibrium MI plateaus. In most optical lattice experiments, the number of atoms (and therefore the signal-to-noise ratio of measurements) is not determined by the number of available atoms from the cooling cycle, but by the available laser power (and therefore beam size) for the optical lattice. This determines the harmonic confinement potential at each lattice depth. The equilibrium size of a MI plateau with n atoms per site is determined by the balance between the local chemical potential $\mu \approx nU$ and the harmonic trapping potential. Its radius $r \propto \mu^{1/2}$, so the total atom number $N \propto U^{3/2}$, where U is controlled by the scattering length a via a Feshbach resonance [34]. We find that the $n = 1$ MI plateau loaded at $a = 300a_0$ has an order of magnitude more atoms than the one loaded at $a = 50a_0$ (see Fig. S3 in Supplemental Material [28]). We initialize the experiment by loading 45 000 atoms at $a = 300a_0$ at a lattice depth $V = 35E_R$ in a pure $n = 1$ MI with diameter of 40–45 sites and then freeze in this distribution by applying a tilt with a 300 μs linear ramp, much faster than $\hbar/t = 28$ ms. This allows the decoupling of MI preparation from further spin experiments, which could be carried out at very different scattering lengths and lattice depths.

(ii) Increasing the speed of superexchange. The speed of superexchange is proportional to t^2 and therefore increases dramatically at lower lattice depths. Because of competing heating and loss processes, most experiments on spin physics are carried out at lattice depths only slightly above the SF-MI transition. The melting of the Mott plateaus at the transition can be suppressed by a tilt, and spin Hamiltonians can be studied at lattice depths even below the phase transition. Next, we experimentally determine how much the lattice depth can be lowered.

We associate the breakdown of the initial MI plateau with the appearance of doublons (two atoms per site [35]), which are measured by interaction spectroscopy. We transfer only atoms in $n = 2$ sites to another hyperfine state by using the interaction-shifted transition frequency, so that atoms in $n = 1$ sites are not affected [34]. After loading, we decrease the scattering length, lower the lattice depth V_z along the direction of the tilt, while keeping $V_x = V_y = 35E_R$, and hold for 10 ms. We detect doublons by ramping V_z back to $35E_R$ on a timescale $\sim \hbar/t$ but

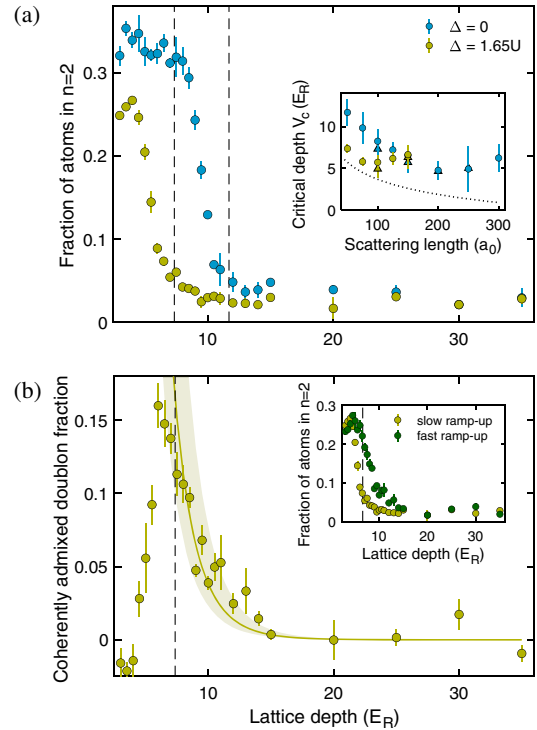


FIG. 2. Stabilization of large Mott plateaus at small lattice depths. (a) Fraction of atoms in doubly occupied sites as a function of lattice depth V_z measured with (gold) and without (blue) a tilt at $a = 50a_0$. (Inset) Critical lattice depth V_c (dashed lines in main plot) below which the fraction of atoms in $n = 2$ is more than 3% above the noise floor. Two initial density distributions are used: (i) nonequilibrium: an $n = 1$ plateau prepared at $a = 300a_0$ (circles), and (ii) equilibrium: an $n = 1$ plateau prepared at the final scattering length (triangles). The dotted line corresponds to the SF-MI transition. (b) Virtual and real doublon populations at $a = 50a_0$ and $\Delta = 1.65U$. The fraction of coherently admixed doublons is the difference between the doublons from the fast and the slow ramp, shown in the inset. (Solid line) Probability of doublon admixture. The shaded region accounts for tilt inhomogeneity. The dashed lines corresponds to V_c . The negative values of the coherent doublon fraction are an artifact in the breakdown regime.

slower than \hbar/U , so that there is local (but not global) equilibrium. The fraction of atoms on $n = 2$ sites at $a = 50a_0$ is shown in Fig. 2(a). Below a critical lattice depth V_c , a sharp increase in the number of doublons is observed. Without the tilt $V_c = 11.7E_R$, while with a tilt of $\Delta = 1.65U$, $V_c = 7.3E_R$, implying an increase in the superexchange rate from Eq. (1) by a factor of 5 at the critical depth in the tilted lattice.

To generalize this result, we repeat the measurement at several scattering lengths [inset of Fig. 2(a)]. All V_c are above the threshold for the SF-MI transition because of the spatial shrinking of the equilibrium Mott plateaus in a harmonic trap [36,37]. Without the tilt, V_c is determined by the proximity to the SF-MI transition and the breakdown of plateaus is driven by first-order tunneling in the single-band

approximation. Note that global density redistribution is not responsible for the breakdown in this measurement, as indicated by the fact that, when the lattice is loaded at the final scattering length, so that little or no density redistribution is expected, we see similar V_c [triangles in Fig. 2(a)].

With the tilt, this melting can be suppressed and we observe that V_c is decreased, resulting in faster spin dynamics. However, we observe that we cannot stabilize the Mott plateaus by tilts for lattice depths smaller than $V_c \approx 6.3E_R$, which we interpret as a breakdown of the single-band approximation. We find V_c to have only a weak dependence on tilt for the range of tilts used ($0.3\text{--}0.9E_R$). Note that, at this lattice depth, the band gap is $3E_R$, and the width of the first excited band is $1.6E_R$. At a somewhat lower lattice depth of $4E_R$, we observe that atoms are accelerated out of the lattice, a clear sign for the breakdown of single-band physics. In cubic 2D and 3D lattices, the motion separates in x , y , and z , and the effective breakdown of the single-band approximation should be independent of dimension. Assuming that the lattice can be lowered to $6.3E_R$ in 3D, then at $a = 100a_0$, where the SF-MI transition is at $V_c = 13.3E_R$, superexchange can be 50 times faster at $\Delta/U = 1.4$, where J/\hbar in Eq. (1) is the same as for $\Delta = 0$.

The tilt suppresses the real population of doublons, responsible for the breakdown of MI plateaus, but not the virtual ones (coherent doublon admixtures), responsible for superexchange. In leading order in perturbation theory in t , the $n = 1$ MI ground state has doublon-hole admixtures with probability $P = 2t^2/(U - \Delta)^2 + 2t^2/(U + \Delta)^2$. These admixtures are taken into account by a unitary transformation which leads to the *effective* spin Hamiltonian acting on the unperturbed states [3,38]. As perturbation theory breaks down when t and U become comparable, the distinction between real and virtual doublons is blurred. Virtual doublons have been detected without a tilt in [39,40]. We measure the number of coherently admixed doublon-hole pairs as the difference between all doublons (measured with a lattice ramp-up faster than \hbar/U , projecting the wave function onto Fock states) and the real doublons [incoherent doublons, measured with a slow, locally adiabatic ramp-up as in Fig. 2(a)]. Figure 2(b) shows that the presence of the tilt does not inhibit this coherent admixture, but only modifies its probability. At V_c , perturbation theory breaks down.

(iii) Tuning the Heisenberg parameters with a tilt. Tilts comparable to U tune the strength and sign of the superexchange interactions [Eq. (1)]. This effect has so far only been observed for two particles in a double well [22]. Here we demonstrate it for the first time in a many-body system by measuring the relaxation dynamics of a nonequilibrium state in a spin chain.

A spin-1/2 Heisenberg model [2] is implemented using the lowest two hyperfine states of ^7Li in a high magnetic field

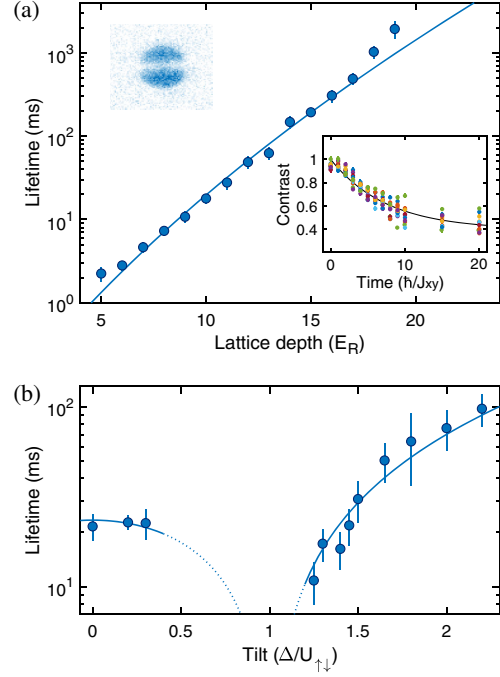


FIG. 3. Relaxation of a nonequilibrium spin pattern by superexchange, controlled by the tilt. (a) Lifetime as a function of lattice depth V_z along the tilt for $\Delta = 1.65U_{\uparrow\downarrow}$. (Inset) Decay of the contrast of the $|\uparrow\rangle$ state for $6E_R \leq V_z \leq 17E_R$. The lifetimes are obtained from exponential fits with an offset. (b) Lifetime as a function of applied tilt at $V_z = 12E_R$. The solid lines in both subfigures are $A\hbar/J_{xy}(\Delta)$, with one fit parameter: (a) $A = 7.54 \pm 0.31$, (b) $A = 6.54 \pm 0.34$. The dotted line indicates the region where the single-band approximation of the Hubbard model breaks down due to resonances of $\Delta = U_{\uparrow\uparrow}, U_{\uparrow\downarrow}, U_{\downarrow\downarrow}$.

$$H = J_z \sum_{\langle i,j \rangle} S_i^z S_j^z + J_{xy} \sum_{\langle i,j \rangle} (S_i^x S_j^x + S_i^y S_j^y), \quad (2)$$

where $\langle i, j \rangle$ denotes nearest neighbors, S_i^α are spin matrices, and J_z and J_{xy} are the superexchange parameters (see Supplemental Material [28]). Similar to [41,42] (our preparation is described in the Supplemental Material [28]), we create a spin pattern and study its relaxation. Using $\pi/2$ pulses and a pulsed magnetic gradient, a spiral spin pattern is created, resulting in a sinusoidal (cosinusoidal) variation of the z (x) projection of the magnetization, which is a superposition of many spin waves (magnons), and is therefore not an eigenstate. The spiral has a pitch of $11.5 \mu\text{m}$, and about two periods fit within the cloud. We measure the relaxation of the spiral by imaging the decaying contrast of the real-space density distribution of $|\uparrow\rangle$ atoms on a CCD camera (with $4 \mu\text{m}$ resolution) in the presence of a tilt $\Delta = 1.65U$.

We first show that the tilt does not inhibit superexchange. To simplify the interpretation, we pick a magnetic field of 848.1014 G at which $J_z = 0$ and the dynamics are solely determined by $J_{xy} = J$ from Eq. (1) with $U = U_{\uparrow\downarrow}$. The inset in Fig. 3(a) shows the decay of the contrast at

several lattice depths, which collapse onto a single curve when the time is rescaled by \hbar/J_{xy} . This confirms, over a range of more than 2 orders of magnitude ($0.015 < J_{xy}/\hbar < 2.68$ kHz), that the spin relaxation is driven by superexchange. We note that the contrast decays to a long-lived offset, which is larger at higher temperatures, probably due to the presence of holes. Also, the offset in the spin-density modulation is smaller than the observed offset in the contrast since our imaging method enhances small contrasts. The dependence of the relaxation time and the offset on parameters of the system, such as the anisotropy of the Heisenberg model, the pitch of the spiral, and temperature, will be addressed in a future study.

We now demonstrate the modification of the superexchange rate with tilt. In general, changing the strength of the tilt also changes the ratio J_z/J_{xy} , which determines the nature of the dynamics and the ground state. For example, when $\Delta > U$, the sign of the Heisenberg parameters can be flipped [see Eqs. (S6) and (S7) in the Supplemental Material [28]], making it possible to go between ferromagnetic and antiferromagnetic coupling. Here we pick a magnetic field of 857.0052 G, at which $U_{\uparrow\uparrow} = -U_{\downarrow\downarrow}$, so that $J_z/J_{xy} = -1$ is constant as a function of tilt. Then, varying the tilt only changes the speed of the dynamics and not the nature of the Hamiltonian. Figure 3(b) shows that the relaxation times can be tuned by the tilt by an order of magnitude ($0.067 < J_{xy}/\hbar < 0.605$ kHz).

(iv) Freezing in defects. A direct consequence of the absence of first-order tunneling in a tilted MI is that defects, which normally propagate at a rate $\sim t/\hbar$, are frozen in. Here we illustrate the different effects of mobile and immobile holes and doublons on the spin transport of a single $|\uparrow\rangle$ atom in a chain of $|\downarrow\rangle$ atoms. We numerically simulate the evolution of the two-component Bose-Hubbard model (see Supplemental Material [28]) for three initial states after tunneling is suddenly switched on. When there are no defects [Figs. 4(a) and 4(d)], the dynamics are the same with and without the tilt. The time evolution of spin $|\uparrow\rangle$ shows coherent ballistic expansion of the wave front with a characteristic checkerboard pattern [43], akin to the dynamics of a single particle in a nontilted lattice [26]. The effect of mobile holes [Fig. 4(b)] is to displace the particles without impeding the overall dynamics significantly, which was also observed for antiferromagnetic chains [44]. Some coherent oscillations appear blurred and are restored by the tilt. In the tilted case, the holes act as domain walls, confining the dynamics to a shorter chain [Fig. 4(e)].

The effect of doublons is more subtle. Compared to holes, the presence of $|\downarrow\downarrow\rangle$ doublons enables the formation of an $|\uparrow\downarrow\rangle$ doublon, so that the $|\uparrow\rangle$ spin can propagate at t/\hbar . Note that due to Bose enhancement, an $|\uparrow\downarrow\rangle$ doublon quickly turns into a $|\downarrow\downarrow\rangle$ doublon. Figure 4(c) shows that the $|\uparrow\rangle$ spin is localized near the original position by collisions with $|\downarrow\downarrow\rangle$ doublons, which we suspect is due to

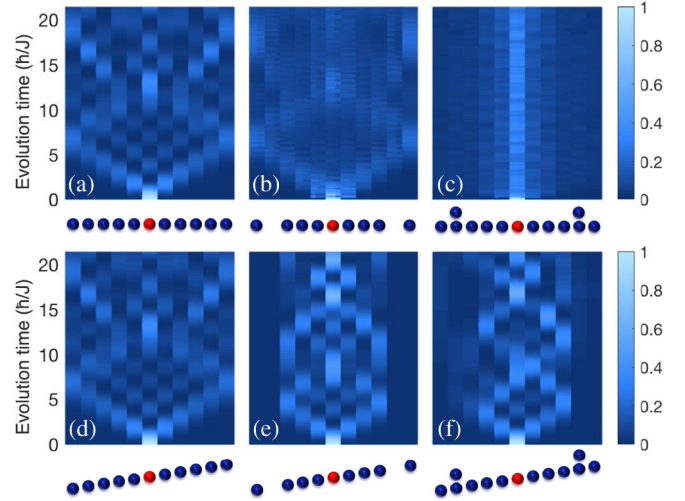


FIG. 4. Effect of holes and doublons on the superexchange dynamics of an $|\uparrow\rangle$ spin in a chain of $|\downarrow\rangle$ spins. Plotted is the probability distribution of the $|\uparrow\rangle$ spin (a)–(c) without and (d)–(f) with the tilt for three initial states: (a),(d) no defects, (b),(e) two holes, (c),(f) two doublons. Here $\Delta = 1.25U$, U is spin independent, and the parameters are chosen so that the superexchange rate J/\hbar is the same as in the case with no tilt.

destructive interference of all paths. With the tilt, doublons are pinned and act as reflective barriers. The superexchange rate for spin $|\uparrow\rangle$ to become part of a doublon is $J_2 = 2t^2[-2/\Delta + 2/(2U_{\uparrow\downarrow} + \Delta)]$, which is different for $\pm\Delta$ and leads to the left-right asymmetry in Fig. 4(f). The effects of fixed and mobile defects in higher dimensions will be somewhat different, but overall, mobile defects can have a significant effect on spin dynamics, while immobile defects act, to a good approximation, as domain walls or static impurities. This has implications not only for dynamics, but also for adiabatic state preparation where the tilt prevents defects from increasing the final entropy (see Fig. S5 in Supplemental Material [28]).

The implementation of tilts for heavier atoms should be less demanding since similar tilts (in units of recoil energy) require lower laser power. Magnetic tilts are also possible if the two spin states have the same magnetic moment. Separation of spin and mass transport could also be achieved with random offsets implemented with bichromatic lattices or laser speckle, as in the studies of Anderson localization [45,46].

We have introduced tilted lattices as a new tool with practical and fundamental applications. On the practical side, we have shown that it can lead to an order of magnitude larger systems with spin-spin couplings that are an order of magnitude faster. On the fundamental side, the tilt can change not only the speed of superexchange, but also the anisotropy of Heisenberg models. It also turns $t - J$ models with mobile holes into spin systems with pinned impurities. This can be used to create lattices with disorder,

similar in spirit to disorder in species-dependent lattices created by pinning the second species [47], and to study mixed-dimensional transport in 2D systems with tilt along one axis [48]. The separation between spin and density dynamics should be useful for future quench experiments and for improving the fidelity of adiabatic preparation of magnetically ordered ground states.

We acknowledge support from the NSF through the Center for Ultracold Atoms and Grant No. 1506369, from ARO-MURI Non-Equilibrium Many-Body Dynamics (Grant No. W911NF-14-1-0003), from AFOSR-MURI Quantum Phases of Matter (Grant No. FA9550-14-1-0035), from ONR (Grant No. N00014-17-1-2253), and from a Vannevar-Bush Faculty Fellowship. Part of this work was done at the Aspen Center for Physics, which is supported by National Science Foundation Grant No. PHY-1607611. We acknowledge support from the EPSRC Programme Grant No. DesOEQ(EP/P009565/1), and by the European Office of Aerospace Research and Development via AFOSR Grant No. FA9550-18-1-0064. Results were obtained using the EPSRC funded ARCHIE-WeSt High Performance Computer (EP/K000586/1).

-
- [1] I. M. Georgescu, S. Ashhab, and F. Nori, *Rev. Mod. Phys.* **86**, 153 (2014).
- [2] L.-M. Duan, E. Demler, and M. D. Lukin, *Phys. Rev. Lett.* **91**, 090402 (2003).
- [3] A. B. Kuklov and B. V. Svistunov, *Phys. Rev. Lett.* **90**, 100401 (2003).
- [4] I. Bloch, *Nat. Phys.* **1**, 23 (2005).
- [5] M. Lewenstein, A. Sanpera, and V. Ahufinger, *Ultracold Atoms in Optical Lattices: Simulating Quantum Many-Body Systems* (Oxford University Press, New York, 2012).
- [6] C. Gross and I. Bloch, *Science* **357**, 995 (2017).
- [7] W. Hofstetter and T. Qin, *J. Phys. B* **51**, 082001 (2018).
- [8] J. Schachenmayer, D. M. Weld, H. Miyake, G. A. Siviloglou, W. Ketterle, and A. J. Daley, *Phys. Rev. A* **92**, 041602(R) (2015).
- [9] C. S. Chiu, G. Ji, A. Mazurenko, D. Greif, and M. Greiner, *Phys. Rev. Lett.* **120**, 243201 (2018).
- [10] J.-S. Bernier, C. Kollath, A. Georges, L. De Leo, F. Gerbier, C. Salomon, and M. Köhl, *Phys. Rev. A* **79**, 061601(R) (2009).
- [11] C. J. M. Mathy, D. A. Huse, and R. G. Hulet, *Phys. Rev. A* **86**, 023606 (2012).
- [12] T.-L. Ho and Q. Zhou, [arXiv:0911.5506](https://arxiv.org/abs/0911.5506).
- [13] A. Mazurenko, C. S. Chiu, G. Ji, M. F. Parsons, M. Kanász-Nagy, R. Schmidt, F. Grusdt, E. Demler, D. Greif, and M. Greiner, *Nature (London)* **545**, 462 (2017).
- [14] H. Miyake, G. A. Siviloglou, C. J. Kennedy, W. C. Burton, and W. Ketterle, *Phys. Rev. Lett.* **111**, 185302 (2013).
- [15] M. Aidelsburger, M. Atala, M. Lohse, J. T. Barreiro, B. Paredes, and I. Bloch, *Phys. Rev. Lett.* **111**, 185301 (2013).
- [16] C. J. Kennedy, W. C. Burton, W. C. Chung, and W. Ketterle, *Nat. Phys.* **11**, 859 (2015).
- [17] M. Aidelsburger, M. Lohse, C. Schweizer, M. Atala, J. T. Barreiro, S. Nascimbène, N. R. Cooper, I. Bloch, and N. Goldman, *Nat. Phys.* **11**, 162 (2015).
- [18] S. Sachdev, K. Sengupta, and S. M. Girvin, *Phys. Rev. B* **66**, 075128 (2002).
- [19] J. Simon, W. S. Bakr, R. Ma, M. E. Tai, P. M. Preiss, and M. Greiner, *Nature (London)* **472**, 307 (2011).
- [20] F. Meinert, M. J. Mark, E. Kirilov, K. Lauber, P. Weinmann, A. J. Daley, and H.-C. Nägerl, *Phys. Rev. Lett.* **111**, 053003 (2013).
- [21] F. Meinert, M. J. Mark, E. Kirilov, K. Lauber, P. Weinmann, M. Gröbner, A. J. Daley, and H.-C. Nägerl, *Science* **344**, 1259 (2014).
- [22] S. Trotzky, P. Cheinet, S. Fölling, M. Feld, U. Schnorrberger, A. M. Rey, A. Polkovnikov, E. A. Demler, M. D. Lukin, and I. Bloch, *Science* **319**, 295 (2008).
- [23] R. C. Brown, R. Wyllie, S. B. Koller, E. A. Goldschmidt, M. Foss-Feig, and J. V. Porto, *Science* **348**, 540 (2015).
- [24] P. A. Lee, N. Nagaosa, and X.-G. Wen, *Rev. Mod. Phys.* **78**, 17 (2006).
- [25] M. Ben Dahan, E. Peik, J. Reichel, Y. Castin, and C. Salomon, *Phys. Rev. Lett.* **76**, 4508 (1996).
- [26] P. M. Preiss, R. Ma, M. E. Tai, A. Lukin, M. Rispoli, P. Zupancic, Y. Lahini, R. Islam, and M. Greiner, *Science* **347**, 1229 (2015).
- [27] I. Dimitrova, W. Lunden, J. Amato-Grill, N. Jepsen, Y. Yu, M. Messer, T. Rigaldo, G. Puentes, D. Weld, and W. Ketterle, *Phys. Rev. A* **96**, 051603(R) (2017).
- [28] See Supplemental Material at <http://link.aps.org/supplemental/10.1103/PhysRevLett.124.043204> for technical details, which includes Refs. [29–33].
- [29] S. Pielawa, T. Kitagawa, E. Berg, and S. Sachdev, *Phys. Rev. B* **83**, 205135 (2011).
- [30] P. Weinberg and M. Bukov, *SciPost Phys.* **2**, 003 (2017).
- [31] P. Weinberg and M. Bukov, *SciPost Phys.* **7**, 020 (2019).
- [32] A. S. Sørensen, E. Altman, M. Gullans, J. V. Porto, M. D. Lukin, and E. Demler, *Phys. Rev. A* **81**, 061603(R) (2010).
- [33] E. Altman, W. Hofstetter, E. Demler, and M. D. Lukin, *New J. Phys.* **5**, 113 (2003).
- [34] J. Amato-Grill, N. Jepsen, I. Dimitrova, W. Lunden, and W. Ketterle, *Phys. Rev. A* **99**, 033612 (2019).
- [35] N. Strohmaier, D. Greif, R. Jördens, L. Tarruell, H. Moritz, T. Esslinger, R. Sensarma, D. Pekker, E. Altman, and E. Demler, *Phys. Rev. Lett.* **104**, 080401 (2010).
- [36] T. D. Kühner and H. Monien, *Phys. Rev. B* **58**, R14741 (1998).
- [37] S. Ejima, H. Fehske, and F. Gebhard, *Europhys. Lett.* **93**, 30002 (2011).
- [38] P. Avan, C. Cohen-Tannoudji, J. Dupont-Roc, and C. Fabre, *J. Phys. (France)* **37**, 993 (1976).
- [39] F. Gerbier, A. Widera, S. Fölling, O. Mandel, T. Gericke, and I. Bloch, *Phys. Rev. Lett.* **95**, 050404 (2005).
- [40] W. S. Bakr, A. Peng, M. E. Tai, R. Ma, J. Simon, J. I. Gillen, S. Fölling, L. Pollet, and M. Greiner, *Science* **329**, 547 (2010).
- [41] A. B. Bardoun, S. Beattie, C. Luciuk, W. Cairncross, D. Fine, N. S. Cheng, G. J. A. Edge, E. Taylor, S. Zhang, S. Trotzky, and J. H. Thywissen, *Science* **344**, 722 (2014).

- [42] S. Hild, T. Fukuhara, P. Schauß, J. Zeiher, M. Knap, E. Demler, I. Bloch, and C. Gross, *Phys. Rev. Lett.* **113**, 147205 (2014).
- [43] T. Fukuhara, A. Kantian, M. Endres, M. Cheneau, P. Schauß, S. Hild, D. Bellem, U. Schollwöck, T. Giamarchi, C. Gross, I. Bloch, and S. Kuhr, *Nat. Phys.* **9**, 235 (2013).
- [44] T. A. Hilker, G. Salomon, F. Grusdt, A. Omran, M. Boll, E. Demler, I. Bloch, and C. Gross, *Science* **357**, 484 (2017).
- [45] G. Roati, C. D'Errico, L. Fallani, M. Fattori, C. Fort, M. Zaccanti, G. Modugno, M. Modugno, and M. Inguscio, *Nature (London)* **453**, 895 (2008).
- [46] J. Billy, V. Josse, Z. Zuo, A. Bernard, B. Hambrecht, P. Lugan, D. Clément, L. Sanchez-Palencia, P. Bouyer, and A. Aspect, *Nature (London)* **453**, 891 (2008).
- [47] U. Gavish and Y. Castin, *Phys. Rev. Lett.* **95**, 020401 (2005).
- [48] F. Grusdt, Z. Zhu, T. Shi, and E. Demler, *SciPost Phys.* **5**, 57 (2018).